



# Effect of nanometer zinc oxide and processing technology on the properties of antibacterial composites

Ying Wang<sup>1,2</sup> · Ting Wang<sup>2</sup> · Li-Zhi Liu<sup>1,2</sup> · Yuanxia Wang<sup>2</sup> · Lixin Song<sup>2</sup> · Ying Shi<sup>2,3</sup> 

Received: 11 April 2023 / Revised: 3 September 2023 / Accepted: 20 October 2023 /  
Published online: 14 November 2023

© The Author(s), under exclusive licence to Springer-Verlag GmbH Germany, part of Springer Nature 2023

## Abstract

With the increasing concern for health and safety, it is crucial to investigate how antibacterial agents demonstrate high antibacterial activity in two-phase blend systems. In this study, we prepared antibacterial films comprising a low concentration (0.2%) zinc oxide/ethylene-octene copolymer (ZnO/POE) and ZnO/linear low-density polyethylene (LLDPE) with high antibacterial activity (99.9%) and an antibacterial property value ( $R$ ) of 6.9. The addition of nanometer (nano) ZnO induces the crystallization of pure materials, increasing their crystallinity and long period and significantly reducing spherulite size. Using a two-phase blending process, we achieved an antibacterial activity of (ZnO/POE)/(ZnO/LLDPE) (0.2%) of 99.9% with an  $R$ -value of 6.9, superior to the single-phase blending of POE/(ZnO/LLDPE) (0.2%) (99.0%,  $R=2.0$ ). Significantly, this difference can be attributed to the fact that nano-ZnO promotes the compatibility of POE and LLDPE in the two-phase blending process. Additionally, the two-phase blending process enhances tear strength and light transmittance compared to single-phase blending. These findings are of great significance for developing nano-ZnO-based two-phase blend antibacterial materials with low concentration and high antibacterial activity.

**Keywords** Nano-zinc oxide · Nanocomposites · Antibacterial activity · Phase behavior

---

✉ Ying Shi  
shiyang86@aliyun.com

<sup>1</sup> School of Materials Science and Engineering, Shenyang University of Technology, Shenyang 110142, China

<sup>2</sup> Advanced Manufacturing Institute of Polymer Industry, Shenyang University of Chemical Technology, Shenyang 110142, China

<sup>3</sup> Research and development, Dongguan HAILI Chemical Material CO., LTD, Dongguan 523000, China

## Introduction

In recent years, antibacterial polymer materials have garnered significant attention in biomedicine [1]. Numerous types of antibacterial polymers have been extensively researched and developed [2, 3]. By incorporating safe and dependable antibacterial agents, these polymer materials demonstrate the ability to inhibit bacterial growth effectively [4, 5]. Nanometer zinc oxide (nano-ZnO) has emerged as a widely used choice in food [6], medical [7], and other industries due to its non-toxicity, persistent activity, low cost, and biocompatibility [8–10]. The antimicrobial properties of nano-ZnO against *Escherichia coli* (*E. coli*) have been extensively studied [11]. For instance, Li et al. [12] incorporated ZnO nanoparticles (0.8%) into linear low-density polyethylene (LLDPE), while Li et al. [13] utilized nano-ZnO (1%) in high-density polyethylene (HDPE) packaging.

Furthermore, careful selection of suitable materials plays a crucial role in the design of medical devices in the field of functional nanocomposites. LLDPE, a semicrystalline polymer, finds wide-ranging applications in manufacturing vital biomedical devices like medical packaging films, medical infusion bags and catheters, owing to its exceptional puncture resistance and flexibility [14–16]. Moreover, the ability of nano-sized ZnO to migrate to the surface of polyolefins is directly proportional to the ultimate antibacterial performance of the composite material. Compared to other ethylene-based polyolefins, LLDPE exhibits a weaker hindered arrangement structure that impedes ZnO migration, resulting in higher antibacterial activity [17]. Ethylene-octene copolymer (POE) offers comprehensive properties such as high elasticity and transparency [18–20]. It demonstrates excellent compatibility with LLDPE and serves as an ideal candidate for enhancing the puncture resistance and elasticity of polyethylene (PE) [21–23]. The thermal properties and phase behavior of LLDPE/POE blends have been extensively studied [24–26].

Polyethylene and its blends are commonly used in biomedical devices due to their excellent cost-effectiveness and desirable functional performance [27]. Some researchers have prepared ZnO/low-density polyethylene (LDPE)/ethylene–vinyl acetate (EVA) (4/100/15) blends for use in antibacterial medical catheters [28]. However, the immiscibility or incompatibility between polyolefins and hydrophilic or polar organic and inorganic compounds can lead to undesirable issues such as aggregation and poor distribution during the blending process [29, 30]. For example, it is common to incorporate 3–5% antimicrobial agents into polymer blends in order to achieve a high level of antimicrobial activity. For instance, Promhuad et al. [31] demonstrated that the addition of 0.9% ZnO resulted in only a slight reduction in microbial growth, whereas the inclusion of 4.5% ZnO effectively inhibited the growth of *Escherichia coli* in PBAT/PBS blends during storage. Shankar and Rhim [32] utilized 3% ZnO to prepare PLA/PBAT antimicrobial composite films with exceptional antimicrobial properties. On the other hand, for non-blended materials, the addition of 0.5–1.5% antimicrobial agents often yields desirable antibacterial effects. Wang et al. [33] obtained satisfactory antibacterial effects using 1% ZnO in PBAT blends. Consequently, achieving excellent

antibacterial performance often necessitates the addition of higher amounts of antibacterial agents. However, the specific mechanism by which antibacterial agents exert their activity in two-phase structures has yet to be fully discussed. Therefore, it is crucial to explore the effects of antibacterial agents on the phase behavior and crystal structure of the two-phase system to enhance the antibacterial efficacy in such systems.

In this paper, we selected a two-phase blend system of LLDPE/POE (80/20) and successfully prepared a two-phase blend antibacterial composite material with high antibacterial activity (99.9%,  $R=6.9$ ) by incorporating a small amount of nano-ZnO as an antibacterial agent. We systematically investigated the impact of nano-ZnO as an antibacterial agent on the phase behavior, crystal structure, and spherical morphology of LLDPE/POE by deliberately controlling its dispersion in different regions of the two-phase system. Furthermore, we explored the variations in mechanical and optical properties induced by nano-ZnO. The findings of this study contribute to a deeper understanding of the development of two-phase blend antibacterial materials, facilitating their further advancements in product development.

## Experimental section

### Materials

The commercial LLDPE (7042N) was sourced from China Petroleum & Chemical Corporation, and the commercial POE (ENGAGE 8480) was purchased from Dow Chemical. The POE is an ethylene-octene copolymer with a 20 wt% octene content. Nano-ZnO ethanol solution (ZnO solid content, 20%) was obtained from Xuancheng Jingrui New Material Co., Ltd. The particle size of the nano-ZnO is 15 nm. The density of nano-ZnO is 5.606 g/cm<sup>3</sup>.

### Preparation of the antibacterial composites

The sample used in this experiment was produced by melt blending with a twin-screw extruder (TDS-20B, Nanjing Norda Extrusion Equipment Co., Ltd., Nanjing, China). The POE/LLDPE blend is prepared by melt blending 20% POE and 80% LLDPE. The antibacterial resin is prepared by combining an antibacterial agent with the substrate material. The ethanol solution of nano-ZnO used in the experiment contains 20% solid ZnO. By melt blending a mass of  $m$  of nano-ZnO ethanol solution with a mass of  $n$  of POE matrix, ZnO/POE masterbatch is prepared. The solid content of nano-ZnO in the ZnO/POE masterbatch, denoted as  $A$ , is calculated as follows:

$$A = (m \times 20\%) / (m \times 20\% + n) \times 100\% \quad (1)$$

where  $m$  is 20 g,  $n$  is 96 g, and after calculation,  $A$  is 4%. The preparation method for the ZnO/LLDPE masterbatch is the same as that for the ZnO/POE masterbatch. The solid content of nano-ZnO in the ZnO/POE masterbatch is 4%. The purpose

of preparing the masterbatch is to facilitate the uniform mixing of nano-ZnO in the substrate. The names and corresponding formulations of the prepared antibacterial resins are listed in Table 1.

The ZnO/POE antibacterial resin is prepared by three rounds of melt blending of the ZnO/POE masterbatch and POE matrix. The solid content of nano-ZnO in the ZnO/POE antibacterial resin is denoted as  $B$ , and it satisfies the equation:

$$B = (4\% \times M_{ZP}) / (M_{ZP} + M_P) \times 100\% \quad (2)$$

In Table 1, the values of  $M_{ZP}$  and  $M_P$  are listed. After calculation,  $B$  is determined to be 0.2%. Similarly, using the same method of preparation, the ZnO/LLDPE antibacterial resin also has a solid content of nano-ZnO denoted as  $C$ , which is 0.2% as well. POE/(ZnO/LLDPE) is prepared by first melt blending the ZnO/LLDPE masterbatch with the LLDPE matrix and then undergoing three rounds of melt blending with the POE matrix. This process is referred to as single-phase blending. The calculation formula for the solid content of nano-ZnO in POE/(ZnO/LLDPE) ( $D$ ) is as follows:

$$D = (4\% \times M_{ZL}) / (M_{ZL} + M_P + M_L) \times 100\% \quad (3)$$

The masses of  $M_{ZL}$ ,  $M_P$ , and  $M_L$  are listed in Table 1. After calculation,  $D$  is determined to be 0.2%. For (ZnO/POE)/(ZnO/LLDPE), the intermediate product “X” is prepared by melt blending the ZnO/POE masterbatch with POE. The intermediate product “Y” is obtained by melt blending the ZnO/LLDPE masterbatch with LLDPE. In both “X” and “Y,” the solid content of nano-ZnO accounts for 0.2% of either “X” or “Y” to ensure uniform dispersion of nano-ZnO. Finally, through three cycles of melt blending, 20% of “X” and 80% of “Y” are mixed together to obtain (ZnO/POE) / (ZnO/LLDPE). This process is referred to as two-phase blending. The calculation formula for the solid content of nano-ZnO in (ZnO/POE) / (ZnO/LLDPE) ( $E$ ) is as follows:

$$E = (4\% \times M_{ZL}) + (4\% \times M_{ZP}) / (M_{ZL} + M_{ZP} + M_P + M_L) \times 100\% \quad (4)$$

The relevant masses are listed in Table 1. After calculation,  $E$  is determined to be 0.2%. Among them, nano-ZnO in POE/(ZnO/LLDPE) is primarily present in the LLDPE phase, accounting for a total mass content of 0.2%. In (ZnO/POE)/(ZnO/

**Table 1** Names and corresponding compositions of antibacterial resins

Mass	Name			
	ZnO/POE	ZnO/LLDPE	POE/(ZnO/LLDPE)	(ZnO/POE)/(ZnO/LLDPE)
ZnO/POE masterbatch ( $M_{ZP}$ )	50 g	0 g	0 g	10 g
ZnO/LLDPE masterbatch ( $M_{ZL}$ )	0 g	50 g	50 g	40 g
POE matrix ( $M_P$ )	950 g	0 g	200 g	190 g
LLDPE matrix ( $M_L$ )	0 g	950 g	750 g	760 g

LLDPE), nano-ZnO is present in both the LLDPE and POE phases. Specifically, in (ZnO/POE)/(ZnO/LLDPE), nano-ZnO carries a content label of 0.2% by weight in the POE phase and an equivalent content label in the LLDPE phase, resulting in a combined total mass content of 0.2%. The nano-ZnO content in all antibacterial resins accounts for 0.2% of the total weight of the material. All samples used in this study are listed in Table 2. The melt index (MI) was determined using the GB/T3682.1-2018 test method, with a 190 °C test temperature and a 2.16 kg load. The MI values are summarized in Table 2.

A plate vulcanizer (QINGDAO YADONG RUBBER MACHINERY CO., LTD. China) was employed to prepare thin films and sheets. The samples were pressed at 5 MPa and 180 °C for 5 min and then kept under the same pressure while rapidly cooling to room temperature. The prepared films were used for antibacterial activity characterization, light transmittance, and tear strength testing. A sheet with a 1-mm thick bottom was prepared using a steel mold for small-angle X-ray diffraction characterization.

### Thermal analysis

The melting behavior and crystallization behavior were characterized by TA Q200 differential scanning calorimeter (DSC) in a nitrogen atmosphere. The sample was first heated to 200 °C for 5 min to eliminate previous thermal mechanical history. Then, it was cooled to 20 °C at a rate of 10 °C/min and reheated back to 200 °C at the same rate. The crystallization temperature ( $T_c$ ), melting temperature ( $T_m$ ), and enthalpy of melting ( $\Delta H_m$ ) were evaluated through non-isothermal crystallization behavior and melting behavior. The normalized crystallinity ( $X_c$ ) of the polyethylene (PE) component was calculated using the following equation:

$$X_c(\%) = \Delta H_m / \varphi \Delta H_m^0 \times 100\% \tag{5}$$

where  $\varphi$  is the weight fraction of PE in the copolymer, and the theoretical melting heat  $\Delta H_m^0$  of 100% crystalline PE is 293 J/g [34].

**Table 2** The melt index (MI) of the materials used

Sample	MI (g/10 min)
POE	1.01
ZnO/POE (0.2%)	1.03
LLDPE	2.07
ZnO/LLDPE (0.2%)	2.11
POE/LLDPE	0.90
POE/(ZnO/LLDPE) (0.2%)	1.68
(ZnO/POE)/(ZnO/LLDPE) (0.2%)	1.64

## Small-angle X-ray scattering (SAXS)

Small-angle X-ray scattering (SAXS) measurements were carried out at the Beijing 1W2A Beamline. The wavelength ( $\lambda$ ) is 0.1542 nm (Cu K  $\alpha$ ). The pixel size of the signal detector (MAR165CCD) is 1024  $\times$  1024 pixels. The distance between the sample and the detector was set at 1665.56 mm. The exposure time was 15 s.

## Small-angle light scattering

The shape and size of spherulites were investigated using a small-angle laser scattering instrument that we built. The experimental setup mainly consisted of five parts: a laser transmitter (Compass 315 M-50, Beijing Laserwave Photoelectric Technology Co., Ltd) with a laser wavelength ( $\lambda$ ) of 520 nm, a polarizer, a rotating sample stage, another polarizer, and a receiving white screen.

The average radius ( $r$ ) of spherulites can be evaluated according to the following formula:

$$r = 4.09\lambda/4\pi \sin \frac{\theta_m}{2} \quad (6)$$

The distance ( $D$ ) between the sample and the receiving screen for the small-angle laser scattering instrument was 5.5 cm. The tangent of the scattering angle  $\theta_m$  was calculated as the ratio of the distance from the center of the scattering pattern to the brightest point of the four lobes ( $L$ ) to the vertical distance of the sample to the image receiving screen ( $D$ ).

## Measurement of the antibacterial activity

The antibacterial activity (AR) of the nano-ZnO composite against *Escherichia coli* (ATCC8739) was determined using the GB/T31402-2015 method. Prior to the experiment, high-temperature sterilization at 120 °C for 5 min was conducted. The sample size was 5\*5 cm<sup>2</sup>. The bacteria were counted using the plate counting method and compared with the number of bacteria in the control sample. The experiment was repeated three times. AR and the antibacterial performance value (R) were evaluated according to GB/T31402-2015 and GB21551.2-2010. The AR and R can be evaluated according to the following formula:

$$AR = (B - C)/B \times 100\% \quad (7)$$

$$R = U_t - A_t \quad (8)$$

where  $B$  represents the number of bacteria adhered to the non-antibacterial sample after 24 h of cultivation, while  $C$  represents the number of bacteria adhered to the antibacterial sample after 24 h of cultivation.  $U_t$  represents the logarithmic mean

of bacterial count (CFU/cm<sup>2</sup>) obtained from the untreated samples after 24 h of inoculation, and  $A_t$  represents the logarithmic mean of bacterial count (CFU/cm<sup>2</sup>) obtained from the antibacterial treated samples after 24 h of inoculation.

### Haze and light transmittance test

The light transmittance and haze were measured according to national standard GB/T2410-2008 using a light transmittance/haze tester (TH-100, Hangzhou Caipu Technology Co., Ltd.). To eliminate the surface haze impact on the measurement of internal haze, a small amount of liquid paraffin was evenly applied on both sides of the flat film and smoothed out.

### The tear strength test

The tear strength of the samples was determined using a universal tensile testing machine (Instron 3365) following the standard method QBT1130-1991. The tear strength was tested with a separation speed of 200 mm/min, and the experiment was repeated five times to obtain the average tear strength.

## Result and discussion

### Effects of nano-ZnO and processing methods on crystallization and thermal behavior of composites

The non-isothermal crystallization behavior of POE, LLDPE, and their corresponding nano-ZnO composites (0.2%) during cooling at a rate of 10 °C/min from melt and subsequent heating at a rate of 10 °C/min was studied using DSC. The details of Fig. 1, including the  $T_c$ ,  $T_m$ , and  $X_c$ , are summarized in Table 3, and the nano-ZnO content in all composites was maintained at a constant 0.2%. Figure 1a demonstrates the crystallization behavior of POE, LLDPE, and the corresponding nano-ZnO composites. The  $T_c$  of LLDPE is 106.1 °C with a crystallinity of 38.1%, which is much higher than that of POE (80.5 °C and 32.3%). These results indicate that the crystallization ability of POE is significantly lower than that of LLDPE. The  $T_c$  of ZnO/POE and ZnO/LLDPE shifts to a higher temperature than pure POE and LLDPE, respectively, suggesting that the ZnO nanoparticles can act as sites for heterogeneous nucleation, resulting in the growth of the POE and LLDPE molecular chains (with nanoparticles as the core) at a higher temperature. Notably, the  $T_c$  of the POE group increased more significantly than that of the LLDPE group, which may be due to the stronger crystallization ability of LLDPE and the less obvious induction effect. The crystallization behavior of POE/LLDPE, POE/(ZnO/LLDPE) (0.2%), and (ZnO/POE)/(ZnO/LLDPE) (0.2%) blends is shown in Fig. 1c. As displayed in the figure, POE/LLDPE and the two kinds of nano-ZnO blends prepared by different processes exhibit two crystallization peaks, with the higher temperature corresponding to the crystallization peak of LLDPE and the lower temperature corresponding

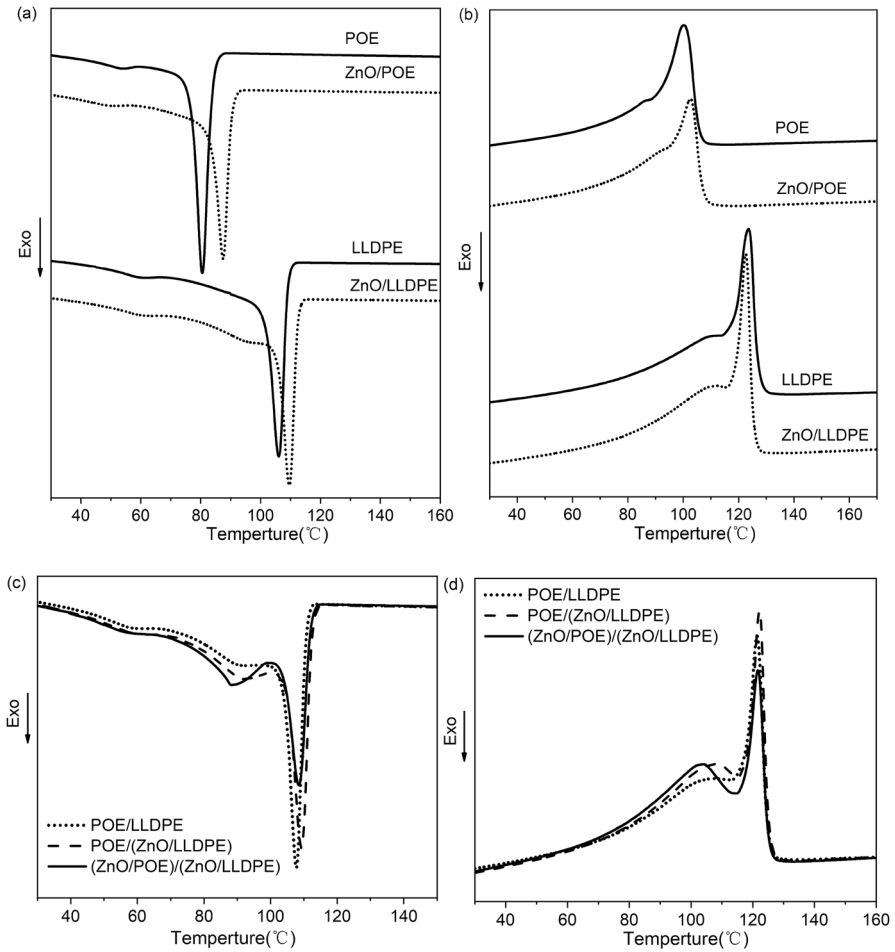


**Fig. 1** DSC cooling curve (**a**, **c**) and heating curve (**b**, **d**) of pure polymers, blend and corresponding nano-ZnO composites

**Table 3** DSC data of pure materials, blends and corresponding nano-ZnO composites

Sample	$T_c$ (°C)	$T_m$ (°C)	$X_c$ (%)
POE	80.5	100.3	32.3
ZnO/POE (0.2%)	87.5	102.6	32.4
LLDPE	106.1	123.6	38.1
ZnO/LLDPE (0.2%)	109.6	122.6	43.6
POE/LLDPE	107.8	121.4	34.9
POE/(ZnO/LLDPE) (0.2%)	109.3	122.2	40.9
(ZnO/POE)/(ZnO/LLDPE) (0.2%)	108.6	121.6	39.4



to that of POE. It is noteworthy that the crystallization peak area of LLDPE in (ZnO/POE)/(ZnO/LLDPE) (0.2%) is significantly smaller than that of POE/LLDPE and POE/(ZnO/LLDPE) (0.2%), while the crystallization peak area of POE increases. This suggests that the crystallization of LLDPE is inhibited while the crystallization of POE is promoted. This is because more POE, influenced by nano-ZnO, enters LLDPE, inhibiting its crystallization, while pre-crystallized LLDPE acts as nucleation sites to promote the crystallization of POE.

Figure 1(b, d) illustrates the secondary heating traces of POE, LLDPE, POE/LLDPE, and their corresponding nano-ZnO composite materials. As shown in Fig. 1b and summarized in Table 3, the  $T_m$  of ZnO/POE is higher than that of pure POE, indicating the formation of some crystals with a larger size. The  $T_m$  of ZnO/LLDPE did not show a significant increase compared to pure LLDPE, indicating that the crystal size did not significantly change. The cause of this phenomenon is the poor crystallization ability of POE, which allows sufficient space for gradual growth as POE crystals develop around the crystal nucleus. In contrast, LLDPE displays a stronger crystallization ability, and the introduction of nano-ZnO results in the formation of numerous crystal nuclei. The LLDPE crystals grow simultaneously around these abundant crystal nuclei, limiting the growth space for LLDPE crystals and thereby restricting the increase in their average size. Furthermore, the crystallinity of ZnO composites is higher than that of the pure materials due to the induced crystallization of nano-ZnO. Additionally, In Fig. 1d, there are two melting peaks for POE/LLDPE and corresponding nano-ZnO composites. The melting peak at approximately 122 °C is contributed by LLDPE, and the melting peak at around 119 °C is caused by POE forming separate crystalline regions due to its poor compatibility with LLDPE. In Fig. 1d, it can be observed that compared to POE/(ZnO/LLDPE) (0.2%) and POE/LLDPE, the area of the main peak (about 122 °C) of (ZnO/POE)/(ZnO/LLDPE) (0.2%) decreased significantly, while the area of the shoulder peak (about 127 °C) increased, and  $T_m$  shifted to the left. This further demonstrates that the content of some large crystals decreases, and the content of small crystals increases. This is because nano-ZnO facilitates the entry of more POE into the LLDPE phase, suppressing the crystallization of LLDPE. Simultaneously, the pre-crystallized LLDPE and nano-ZnO promote the crystallization of POE, leading to a finer grain size.

### Effect of nano-ZnO and processing technology on microstructure of composites

Figure 2(a, b) shows the linear SAXS profiles for POE, LLDPE, and ZnO composites at room temperature. A scattering peak is observed around  $q=0.3 \text{ nm}^{-1}$  or  $0.4 \text{ nm}^{-1}$ , respectively, corresponding to the long period for polyolefin lamellar stacks. The less ordered scattering from the nano-ZnO composites of pure polymers can be attributed to the impact of the scattering signal of the inorganic nano-ZnO particles at low  $q$ . The averaged interlamellar distance (long period) of the materials can be obtained from the Lorentz-corrected SAXS scattering profiles, as demonstrated in Fig. 2b. It can be observed that the scattering peak for ZnO/POE and ZnO/LLDPE is located at a smaller  $q$  value than that of the corresponding pure

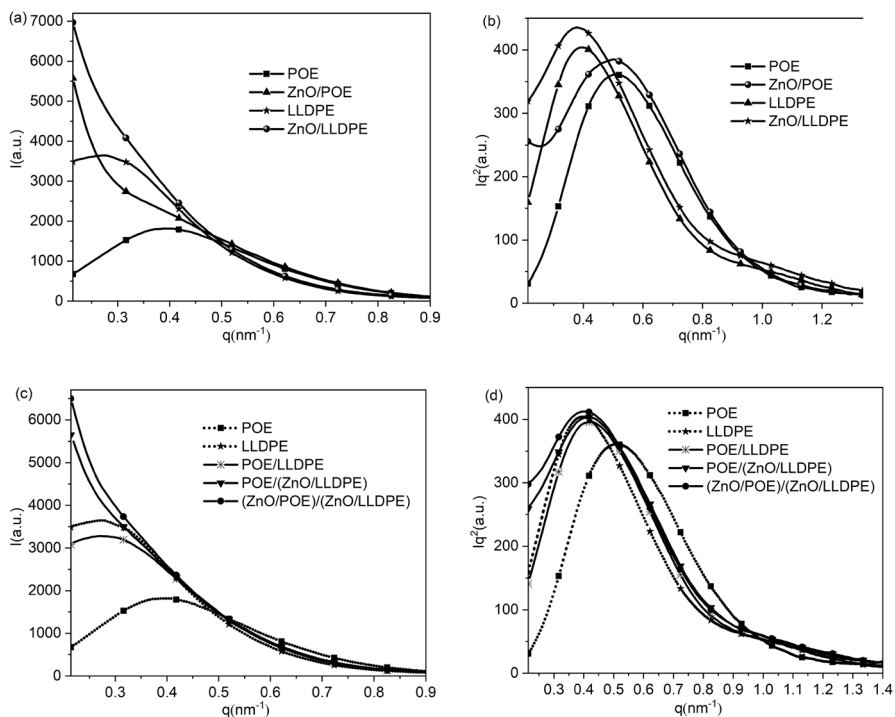


**Fig. 2** Linear (a, c) and Lorentz-corrected (b, d) SAXS profiles of pure polymers, blend and corresponding nano-ZnO composites

**Table 4** The results of long period (L), lamellar size (Lc) and amorphous region size (La)

Sample	L (nm)	Lc (nm)	La (nm)
POE	11.95	5.65	6.30
ZnO/POE (0.2%)	12.62	5.92	6.70
LLDPE	16.13	6.85	9.28
ZnO/LLDPE (0.2%)	16.28	6.91	9.37
POE/LLDPE	14.60	6.68	7.92
POE/(ZnO/LLDPE) (0.2%)	14.93	6.87	8.06
(ZnO/POE)/(ZnO/LLDPE) (0.2%)	15.43	6.86	9.57

polymer, which indicates a larger average long period for the nano-ZnO composites of pure polymers. In Table 4, it can be observed that the addition of nano-ZnO leads to a greater change in the amorphous thickness of both POE and LLDPE. This can be attributed to the distribution of 15 nm nano-ZnO particles, which typically fall within the range of 6–28 nm [36]. Some of these smaller particles are able to enter the amorphous regions, thereby increasing the amorphous region size (La). After the addition of ZnO, the lamellar size (Lc) of POE significantly increased, while the lamellar size (Lc) of LLDPE did not show a significant increase, which is consistent

with the crystal size changes observed in DSC analysis. Higher scattering intensity is also observed for ZnO/POE and ZnO/LLDPE (Fig. 2b), likely due to the greater density difference between neighboring polyolefin crystal lamella and amorphous lamellae, caused by increased density in the amorphous region with the addition of nano-ZnO.

SAXS studies were conducted for POE/LLDPE blends and the corresponding nano-ZnO blend composites, and the results are shown in Fig. 2c. The SAXS scattering peak of the POE/LLDPE blend is located between the peaks of pure POE and pure LLDPE, contributed by both components. The evaluated long period for POE/LLDPE, as listed in Table 4, is 14.6 nm. Due to the similarity in repeating units between LLDPE and POE, their molecular interactions are identical. However, due to differences in molecular structure, the LLDPE/POE blend system exhibits partial compatibility. Assuming a model for partially compatible two-phase polymers, the dispersed phase is distributed at various scales within the continuous phase, while a compatible region, known as the interface layer, forms at the boundary between the dispersed phase and the continuous phase. The thickness of this interface layer in both phases can be determined using the Porod law, which relies on SAXS test results [36]. In an ideal system with well-defined phase boundaries, i.e., an incompatible polymer blend, there is no affinity at the interface. Hence, at the tail end of the scattering curve at large scattering angles, the intensity follows the following formula:

$$\lim_{S \rightarrow \infty} S^4 I(S) = k \tag{9}$$

Here  $S = 4\pi \sin\theta/\lambda$ , where  $\lambda$  is the wavelength, and  $\theta$  is half of the scattering angle.  $k$  is the Porod constant, an important parameter related to structure, and  $I(S)$  is the scattering intensity function corrected by slit collimation. If the interface between the two phases in the system is not well-defined, i.e., the interface is blurred, or there exists an interfacial layer, then the Porod law can be corrected as follows:

$$\lim_{S \rightarrow \infty} S^4 I(S) = k \exp(-\sigma^2 S^2) \tag{10}$$

where  $\sigma$  is the thickness of the interfacial layer between the two phases. Figure 3 represents the  $\ln(S^4 I(S)) - S^2$  curve for both the blend and the corresponding composite material with ZnO. At larger values of  $S$ , a straight line with a certain slope should be obtained. The slope of the line can be used to determine the value of  $\sigma$ , representing the thickness of the interfacial layer. After performing calculations, it was determined that the minimum value of  $\sigma$  for POE/LLDPE is 2.02. The values of  $\sigma$  for POE/(ZnO/LLDPE) (0.2%) and (ZnO/POE)/(ZnO/LLDPE) (0.2%) are 2.09 and 2.16, respectively. The thicker interfacial layer in (ZnO/POE)/(ZnO/LLDPE) (0.2%) suggests a more uniform interface region, resulting in reduced scattering caused by sharp interfaces. To eliminate the influence of nano-ZnO at low  $q$ , the curve after Lorentz transformation is presented in Fig. 2d. Interestingly, even though having the same ZnO content (0.2%), the increased intensity of the scattering peak and broadening of the peak shape of the  $q - iq^2$  curve for (ZnO/POE)/(ZnO/LLDPE) (0.2%) compared to POE/(ZnO/LLDPE) (0.2%) indicates that the crystal arrangement of

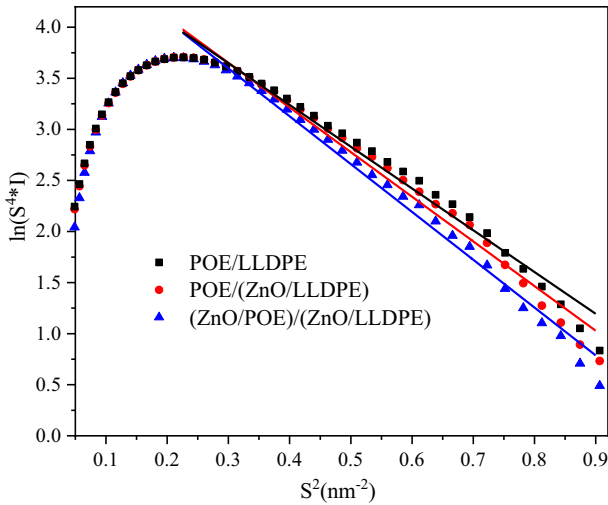


**Fig. 3** Plot of  $\ln(S^{4*}I)$  vs.  $S^2$  for blend and corresponding nano-ZnO composites

(ZnO/POE)/(ZnO/LLDPE) (0.2%) is more disordered due to the good compatibility of the two-phase blending process. In addition, the increase in the size of the amorphous region ( $L_a$ ) listed in Table 4 indicates that nano-ZnO has a greater impact on the amorphous region. Therefore, the compatibility of nano-ZnO-based POE/LLDPE composites processed by the two-phase blending process is significantly enhanced despite having the same content of ZnO. These findings underscore the ability of nano-ZnO to enhance the compatibility between POE and LLDPE under two-phase blending processes.

### Effect of nano-ZnO and processing technology on the morphology of composite spherulites

For regular spherulites, the characteristic pattern of a "four-leaf clover" can be obtained in the Hv mode of laser scattering. As shown in Fig. 4, all samples form a "four-leaf clover" pattern, indicating that these materials form spherulites with different sizes and regularity. The size of the spherulites can be calculated using Eq. (6). In Fig. 3, the maximum spherulite size of pure POE is 8.93  $\mu\text{m}$ , and the spherulite sizes of LLDPE and POE/LLDPE are 2.99  $\mu\text{m}$  and 3.63  $\mu\text{m}$ , respectively. Compared to the sample without nano-ZnO, the nano-ZnO composite has a larger spherulite pattern and more blurred edges, indicating that the spherulite regularity of the formed composite is worse. The spherulite size (2.10  $\mu\text{m}$ ) of (ZnO/POE)/(ZnO/LLDPE) (0.2%) is smaller than that of POE/LLDPE and POE/(ZnO/LLDPE) (0.2%), which may be due to better interface compatibility between POE and LLDPE, resulting in restrained growth of the spherulites in (ZnO/POE)/(ZnO/LLDPE) (0.2%). These results highlight how nano-ZnO can enhance the compatibility between POE and LLDPE under two-phase blending processes.

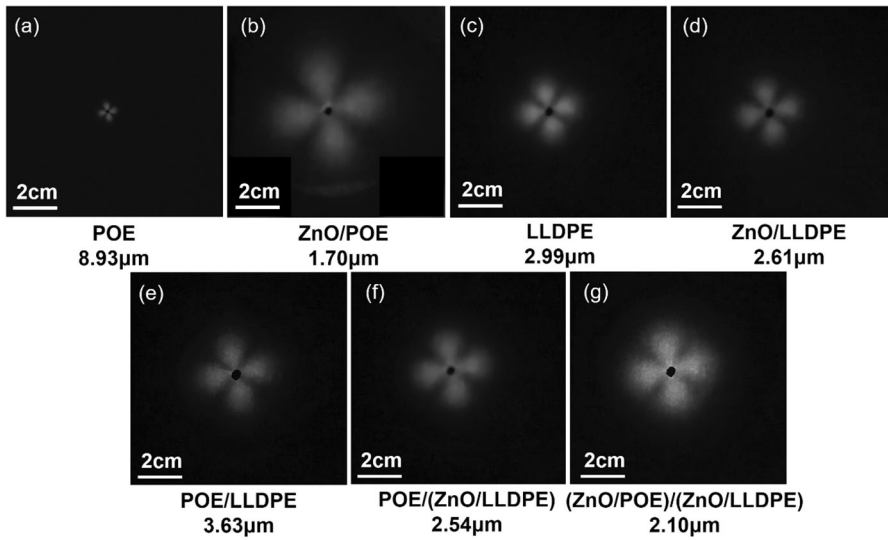


**Fig. 4** Spherulite morphologies of **a** POE, **b** ZnO/POE, **c** LLDPE, **d** ZnO/LLDPE, **e** POE/LLDPE, **f** POE/(ZnO/LLDPE) (0.2%), **g** (ZnO/POE)/(ZnO/LLDPE) (0.2%)

### Effect of nano-ZnO and processing technology on antibacterial activity of composite materials

The antibacterial activity of the nano-ZnO composite film against *E. coli* was evaluated by testing the film surface with the antibacterial activity test. According to GB21551.2-2010, an antibacterial rate of  $\geq 90\%$  indicates a significant antibacterial effect. As shown in Table 5, at a concentration of 0.2% nano-ZnO, the antibacterial rate of ZnO/POE and ZnO/LLDPE was 99.9% with an *R*-value of 6.9. Here, the *R*-value represents the antibacterial effectiveness with multiple "9"s. If the *R*-values of two materials differ by 2, in reality, the difference in the quantity and capability of eradicating *E. coli* is of the magnitude of  $10^2$ . Therefore, both composite materials have achieved a high level of antibacterial activity. Previous researchers added 0.8% ZnO (50 nm) to prepare ZnO/LLDPE composite films with similar size of ZnO on the film surface and obtained 91.7% antibacterial activity [12]. In the experiment described in reference [12], researchers

**Table 5** Antibacterial rate and the *R* of nano-ZnO blends

Sample	Antibacterial rate (%)	<i>R</i>
ZnO/POE (0.2%)	99.9	6.9
ZnO/LLDPE (0.2%)	99.9	6.9
POE/(ZnO/LLDPE) (0.2%)	99.0	2.0
(ZnO/POE)/(ZnO/LLDPE) (0.2%)	99.9	6.9

utilized larger-sized ZnO particles with a diameter of approximately 50 nm, and there were about 220 ZnO particles per gram of ZnO/LLDPE resin. In our experiment, we used ZnO particles with a smaller size of approximately 15 nm, and there were around 2000 of these particles per gram of ZnO/LLDPE resin. Adding smaller-sized nano-ZnO particles results in a higher number of particles being dispersed within the antibacterial film. This facilitates a more uniform distribution of ZnO within the base material, thereby enhancing the antibacterial activity of the ZnO composite material. The antibacterial activity results of POE/LLDPE nano-ZnO composites prepared using different processes are presented in Table 5. It was found that the antibacterial activity of (ZnO/POE)/(ZnO/LLDPE) (0.2%) was 99.9%, with an R-value of 6.9, which is significantly higher than that of POE/(ZnO/LLDPE) (0.2%) (nearly  $10^5$  times higher). In the case of POE/(ZnO/LLDPE) (0.2%) prepared through a single-phase blending process, most of the nano-ZnO particles are present in the LLDPE phase and then migrate to the POE phase. Due to the immiscibility between LLDPE and POE, the migration of nano-ZnO is influenced by the compatibility between the two phases, resulting in a low content of nano-ZnO in the POE phase (Fig. 5). In the antibacterial activity test on the surface of composite films, the dimensions of the film samples were  $5 \times 5 \text{ cm}^2$ . To achieve excellent antibacterial performance, it is necessary to ensure a uniform distribution of a sufficient quantity of nano-ZnO particles across the entire surface of the film. This uneven distribution of nano-ZnO on the surface of the POE/(ZnO/LLDPE) (0.2%) film significantly reduces its antibacterial ability compared to the ZnO/LLDPE composite. On the other hand, (ZnO/POE)/(ZnO/LLDPE) (0.2%) achieves an improved uniform distribution of nano-ZnO particles by employing a two-phase blending approach, thereby obtaining the same high level of antibacterial activity as ZnO/LLDPE (Fig. 4). In fact, in actual industrial production, the two-phase blending process is highly effective in reducing the use of antibacterial agents and achieving even better antibacterial activity.

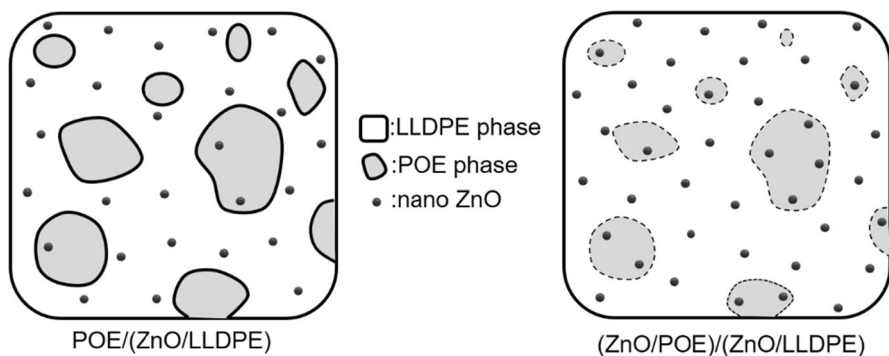


**Fig. 5** Phase region images of POE/(ZnO/LLDPE) (0.2%) and (ZnO/POE)/(ZnO/LLDPE) (0.2%)

### Effect of nano-ZnO and processing technology on optical properties of composites

The internal haze of the film is a thickness-normalized value, and the measurement of the surface haze is not affected by the film thickness. Table 6 shows that the haze of POE is 0.87% lower, while that of LLDPE is 16.56% higher, which is due to the difference in crystallinity (Table 3). The light transmittance of POE is 92.3%, which is higher than that of LLDPE at 90.4%. This is due to the introduction of long branch chains in the main chain of POE to improve material transparency. Compared with pure material, the light transmittance of the nano-ZnO composite is reduced. This is because the addition of nano-ZnO particles with a higher refractive index causes greater scattering loss and lowers light transmission of the film. The increase in internal haze of ZnO/POE and ZnO/LLDPE is due to the increase in internal defects of the film caused by nano-ZnO. Similarly, the internal haze of POE/(ZnO/LLDPE) (0.2%) increases and the transmittance decreases compared to POE/LLDPE due to the addition of nano-ZnO. The difference is that the haze of (ZnO/POE)/(ZnO/LLDPE) (0.2%) is lower than that of POE/(ZnO/LLDPE) (0.2%), which may be due to the good compatibility between POE and LLDPE. Although the haze of (ZnO/POE)/(ZnO/LLDPE) (0.2%) is also higher than that of POE/LLDPE, the addition of nano-ZnO through two-phase blending helps improve compatibility, reduce haze, and increase light transmittance compared to single-phase blending.

### Effect of nano-ZnO and processing technology on tear properties of composites

The tear strength of the sample films is presented in Table 7. The tear strength of the pure sample nano-ZnO composite films is weaker compared to the pure polymer, as shown in Table 7. This decrease in tear strength is attributed to the poor interface bonding between the nano-ZnO and the matrix. Similarly, the tear strength of POE/(ZnO/LLDPE) (0.2%) is lower than that of POE/LLDPE due to the uneven dispersion of nano-ZnO in the matrix. However, it is noteworthy that the tear strength of (ZnO/POE)/(ZnO/LLDPE) (0.2%) is better than that of POE/LLDPE (158.78 N/mm vs. 148.48 N/mm) due to the good compatibility of POE and LLDPE in (ZnO/POE)/(ZnO/LLDPE) (0.2%) and the uniform dispersion of nano-ZnO in the matrix. This further indicates that when using a two-phase blending process, nano-ZnO can act

**Table 6** Haze and transmittance of pure materials, blends and corresponding nano-ZnO composites

Sample	Normalized internal haze (%)	Transmittance (%)
POE	0.87	92.3
ZnO/POE (0.2%)	1.37	91.5
LLDPE	16.56	90.4
ZnO/LLDPE (0.2%)	23.46	89.9
POE/LLDPE	12.94	90.6
POE/(ZnO/LLDPE) (0.2%)	16.08	90.3
(ZnO/POE)/(ZnO/LLDPE) (0.2%)	14.83	90.4

**Table 7** Tear strength of pure materials and corresponding nano-ZnO composites

Sample	Tear strength (N/mm)
POE	104.68
ZnO/POE	96.12
LLDPE	209.73
ZnO/LLDPE	166.06
POE/LLDPE	148.48
POE/(ZnO/LLDPE)	146.64
(ZnO/POE)/(ZnO/LLDPE)	158.78

as a compatibilizer of POE and LLDPE, thereby improving the tear strength of antibacterial materials.

## Conclusions

This study investigated the effects of nano-ZnO and its processing technology on the phase behavior, crystal structure and properties of antibacterial composite materials. In this article, antibacterial films of ZnO/POE and ZnO/LLDPE were prepared with a low concentration of nano-ZnO (0.2%) and exhibited high antibacterial activity (99.9%,  $R=6.9$ ). Nano-ZnO induces crystallization of pure materials, increasing crystallinity and long period. The spherulite size of the nano-ZnO-based pure materials significantly decreased. However, the light transmittance and tear strength of pure materials were reduced by the influence of nano-ZnO.

Through further investigation of the thermal behavior, lamellar structure, and spherulite size of nano-ZnO-based POE/LLDPE antibacterial composites prepared by different processes (two-phase mixing and single-phase blending), it was found that the melting and crystallization peaks of LLDPE decreased significantly, while those of POE increased. The lamellar stacking of (ZnO/POE)/(ZnO/LLDPE) (0.2%) was more disordered, and the spherulite size was smaller compared to POE/(ZnO/LLDPE) (0.2%). At the same time, the antibacterial ability of ZnO/POE/(ZnO/LLDPE) (0.2%) (99.9%,  $R=6.9$ ) was significantly superior to POE/(ZnO/LLDPE) (0.2%) (99.0%,  $R=2.0$ ). Nano-ZnO-based POE/LLDPE blends produced by the two-phase blending process showed better light transmittance and tear strength than those produced by the single-phase blending process. Therefore, a new hypothesis was proposed that nano-ZnO can improve the compatibility of POE and LLDPE through a two-phase blending process. This provides a new way to develop antibacterial blends with excellent comprehensive properties.

**Acknowledgements** Synchrotron SAXS experiments were performed on Beamline 1W2A at the Beijing Synchrotron Radiation Facility. The authors are grateful to the assistance of the beamline scientists at BSRF and SSRF, especially Zhihong Li and Guang Mo.

**Funding** This work is supported by a Liaoning climbing scholar program.



## Declarations

**Conflict of interest** The authors have no competing interests to declare that are relevant to the content of this article.

## References

1. Wang CY, Makvandi P, Zare EN, Tay FR, Niu LN (2020) Advances in antimicrobial organic and inorganic nanocompounds in biomedicine. *Adv Therap* 3(8):2000024. <https://doi.org/10.1002/adtp.202000024>
2. Lam SJ, Wong EH, Boyer C, Qiao GG (2018) Antimicrobial polymeric nanoparticles. *Prog Polym Sci* 76:64–64. <https://doi.org/10.1016/j.progpolymsci.2017.07.007>
3. Zhong Y, Godwin P, Jin Y, Xiao H (2019) Biodegradable polymers and green-based antimicrobial packaging materials: a mini-review. *Adv Inds Eng Poly Res* 3(1):27–35. <https://doi.org/10.1016/j.aiepr.2019.11.002>
4. Ahmad SS, Yousuf O, Islam RU, Younis K (2021) Silver nanoparticles as an active packaging ingredient and its toxicity. *Packag Technol Sci* 34(11–12):653–663. <https://doi.org/10.1002/pts.2603>
5. Dobrucka R, Ankiel M (2019) Possible applications of metal nanoparticles in antimicrobial food packaging. *J Food Safety* 39(2):e12617. <https://doi.org/10.1111/jfs.12617>
6. Bumbudsanpharoke N, Choi J, Park HJ, Ko S (2019) Zinc migration and its effect on the functionality of a low density polyethylene-ZnO nanocomposite film. *Food Packag Shelf* 20:100301. <https://doi.org/10.1016/j.fpsl.2019.100301>
7. Valerini D, Tammaro L, Villani F, Rizzo A, Caputo I, Paoletta G, Vigliotta G (2020) Antibacterial Al-doped ZnO coatings on PLA films. *J Mater Sci* 55(11):4830–4847. <https://doi.org/10.1007/s10853-019-04311-z>
8. Gedik G, Aksit A, Engin B, Paksu U (2018) Production of metal oxide containing antibacterial coated textile material and investigation of the mechanism of action. *Fiber Polym* 19:2548–2563. <https://doi.org/10.1007/s12221-018-8306-9>
9. Ma G, Liang X, Li L, Qiao R, Jiang D, Ding Y, Chen H (2014) Cu-doped zinc oxide and its polythiophene composites: preparation and antibacterial properties. *Chemosphere* 100:146–151. <https://doi.org/10.1016/j.chemosphere.2013.11.053>
10. Naskar A, Lee S, Kim KS (2020) Antibacterial potential of Ni-doped zinc oxide nanostructure: comparatively more effective against gram-negative bacteria including multi-drug resistant strains. *RSC Adv* 10(3):1232–1242. <https://doi.org/10.1039/C9RA09512H>
11. Li M, Zhu L, Lin D (2011) Toxicity of ZnO nanoparticles to *Escherichia coli*: mechanism and the influence of medium components. *Environ Sci Technol* 45(5):1977–1983. <https://doi.org/10.1021/es102624t>
12. Li SC, Li B, Qin ZJ (2010) The Effect of the Nano-ZnO concentration on the mechanical, antibacterial and melt rheological properties of LLDPE/modified nano-ZnO composite films. *Polym Plast Technol* 49(13):1334–1338. <https://doi.org/10.1080/03602559.2010.496431>
13. Li SC, Li YN (2010) Mechanical and antibacterial properties of modified nano-ZnO/high-density polyethylene composite films with a low doped content of nano-ZnO. *J Appl Polym Sci* 116:2965–2969. <https://doi.org/10.1002/app.31802>
14. Liu H, Li SC, Liu Y, Iqbal M (2011) Thermo-stimulative shape memory effect of linear low-density polyethylene/polypropylene (LLDPE/PP) blends compatibilized by crosslinked LLDPE/PP blend (LLDPE-PP). *J Appl Polym Sci* 122(4):2512–2519. <https://doi.org/10.1002/app.34345>
15. Bekhit M, El-Sabbagh SH, Mohamed RM, El-Sayyad GS, Sokary R (2022) Mechanical, thermal and antimicrobial properties of LLDPE/EVA/MMT/Ag nanocomposites films synthesized by gamma irradiation. *J Inorg Organomet* 32:631–645. <https://doi.org/10.1007/s10904-021-02137-4>
16. Bui HT, Prawel DA, Harris KL, Li E, James SP (2019) Development and fabrication of vapor cross-linked hyaluronan-polyethylene interpenetrating polymer network as a biomaterial. *ACS Appl Mater Interfaces* 11(21):18930–18941. <https://doi.org/10.1021/acsami.9b03437>
17. Wang Y, Liu LZ, Tian C, Wang Y, Song L, Shi Y (2023) Crystallization, morphology, optical properties, tear properties and antibacterial properties of nano zinc oxide composites. *J Polym Res* 30(9):352. <https://doi.org/10.1007/s10965-023-03720-8>
18. Lin B, Zheng C, Zhu QY, Xie F (2019) A polyolefin encapsulant material designed for photovoltaic modules: from perspectives of peel strength and transmittance. *J Therm Anal Calorim* 140:2259–2265. <https://doi.org/10.1007/s10973-019-09006-w>

19. Xie TT, Wu H, Bao WT, Guo SY, Chen Y, Huang H, Chen HY, Lai SY, Jow J (2010) Enhanced compatibility of PA6/POE blends by POE-g-MAH prepared through ultrasound-assisted extrusion. *J Appl Polym Sci* 118:1846–1852. <https://doi.org/10.1002/app.32547>
20. Peng H, Lu M, Lv F, Niu M, Wang W (2019) Understanding the effect of silane crosslinking reaction on the properties of PP/POE blends. *Polym Bull* 76:6413–6428. <https://doi.org/10.1007/s00289-019-02724-z>
21. Wang Z, Wang L, Wang X, Hao C (2012) Deformation reversibility enhancement of thermoplastic vulcanizates based on high density polyethylene and ethylene-propylene-diene terpolymer. *Mater Chem Phys* 134(2–3):1185–1189. <https://doi.org/10.1016/j.matchemphys.2012.04.019>
22. Liu S, Wang K, Zhang Z, Ren Y, Chen L, Sun X, Liang W (2020) Effects of ethylene-octene copolymer (POE) on the brittle to ductile transition of high-density polyethylene/POE blends. *Polym Eng Sci* 60(10):2640–2652. <https://doi.org/10.1002/pen.25532>
23. Li Y, Zhang Y, Zhang YX (2003) Structure and mechanical properties of SRP/HDPE/POE (EPR or EPDM) composites. *Polym Test* 22(8):859–865. [https://doi.org/10.1016/S0142-9418\(03\)00022-9](https://doi.org/10.1016/S0142-9418(03)00022-9)
24. Ke QQ, Huang XY, Wei P, Wang GL, Jiang PK (2007) Thermal, mechanical, and dielectric behaviors of crosslinked linear low density polyethylene/polyolefin elastomers blends. *J Appl Polym Sci* 104(3):1920–1927. <https://doi.org/10.1002/app.25874>
25. Kumar P, Narayan Maiti U, Sikdar A, Kumar Das T, Kumar A, Sudarsan V (2019) Recent advances in polymer and polymer composites for electromagnetic interference shielding: review and future prospects. *Polym Rev* 59(4):687–738. <https://doi.org/10.1080/15583724.2019.1625058>
26. Samarth N, Mahanwar P (2018) Study and characterization of LLDPE/polyolefin elastomer and LLDPE/EPDM blend: effect of chlorinated water on blend performance. *Mater Today* 5(10):22433–22446. <https://doi.org/10.1016/j.matpr.2018.06.613>
27. Paxton NC, Allenby MC, Lewis PM, Woodruff MA (2019) Biomedical applications of polyethylene. *Eur Polym J* 118:412–428. <https://doi.org/10.1016/j.eurpolymj.2019.05.037>
28. Galli R, Hall MC, Breitenbach ER, Colpani GL, Zanetti M, de Mello JMM, Fiori MA (2020) Antibacterial polyethylene-ethylene vinyl acetate polymeric blend by incorporation of zinc oxide nanoparticles. *Polym Test* 89:106554. <https://doi.org/10.1016/j.polymertesting.2020.106554>
29. Jeong S, Kim D, Seo J (2015) Preparation and antimicrobial properties of LDPE composite films melt-blended with polymerized urushiol powders (YPUOH) for packaging applications. *Prog Org Coat* 85:76–83. <https://doi.org/10.1016/j.porgcoat.2015.03.012>
30. Soleimani A, Farahmandghavi F, Morshedjan J, Keyvan Rad J (2023) Silver/hydrogen-exchanged zeolites embedded in modified polyethylene blends for antibacterial packaging with prolonged color stability. *ACS Appl Polym Mater* 5(4):2917–2930. <https://doi.org/10.1021/acsapm.3c00126>
31. Promhuad K, Phothisarattana D, Laorenza Y, Bumbudsanpharoke N, Harnkarnsujarit N (2023) Zinc oxide enhanced the antibacterial efficacy of biodegradable PBAT/PBS nanocomposite films: morphology and food packaging properties. *Food Biosci* 55:103077. <https://doi.org/10.1016/j.fbio.2023.103077>
32. Shankar S, Rhim JW (2019) Effect of types of zinc oxide nanoparticles on structural, mechanical and antibacterial properties of poly (lactide)/poly (butylene adipate-co-terephthalate) composite films. *Food Packag Shelf* 21:100327. <https://doi.org/10.1016/j.fpsl.2019.100327>
33. Wang T, Shi Y, Li Y, Liu L (2021) The effects of ZnO nanoparticle reinforcement on thermostability, mechanical, and optical properties of the biodegradable PBAT film. *J Polym Eng* 41(10):835–841. <https://doi.org/10.1515/polyeng-2021-0150>
34. Wang S, Wu C, Ren MQ, Van Horn RM, Graham MJ, Han CC, Cheng SZ (2009) Liquid-liquid phase separation in a polyethylene blend monitored by crystallization kinetics and crystal-decorated phase morphologies. *Polymer* 50(4):1025–1033. <https://doi.org/10.1016/j.polymer.2008.12.028>
35. Zamiri R, Zakaria A, Ahangar HA, Darroudi M, Zak AK, Drummen GP (2012) Aqueous starch as a stabilizer in zinc oxide nanoparticle synthesis via laser ablation. *J Alloy Compd* 516:41–48. <https://doi.org/10.1016/j.jallcom.2011.11.118>
36. Wu T, Li Y, Wu G (2005) Crystalline structure and phase structure of mLLDPE/LDPE blends. *Polymer* 46(10):3472–3480. <https://doi.org/10.1016/j.polymer.2005.02.084>

**Publisher's Note** Springer Nature remains neutral with regard to jurisdictional claims in published maps and institutional affiliations.

Springer Nature or its licensor (e.g. a society or other partner) holds exclusive rights to this article under a publishing agreement with the author(s) or other rightsholder(s); author self-archiving of the accepted manuscript version of this article is solely governed by the terms of such publishing agreement and applicable law.